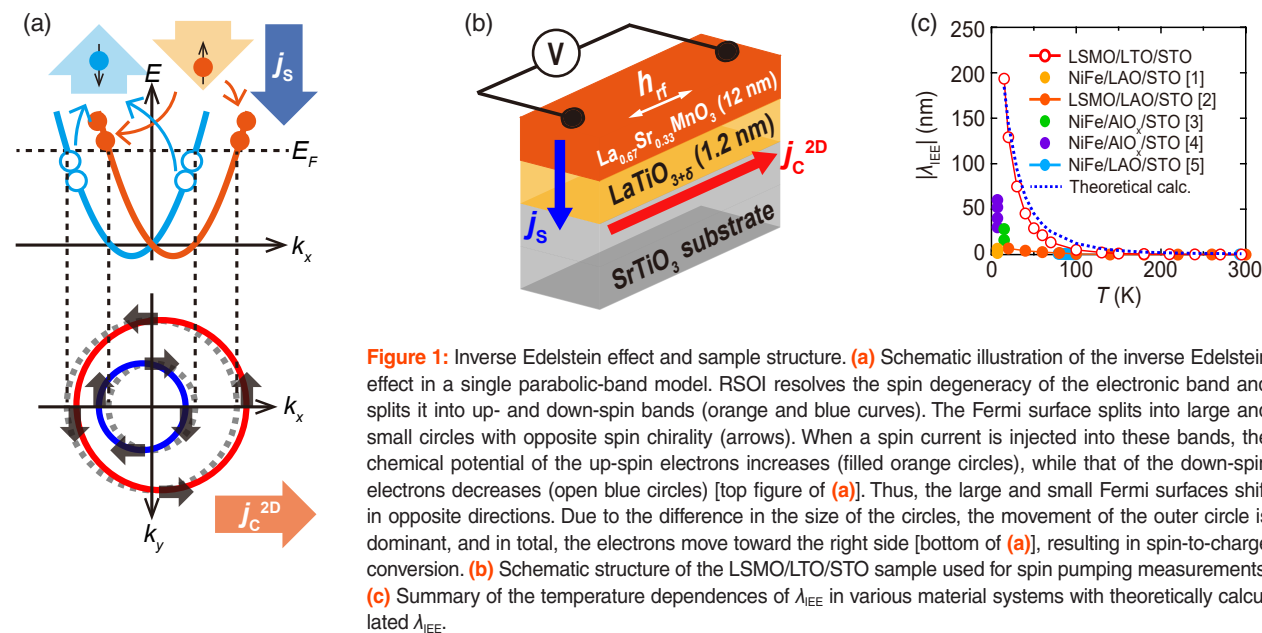


## Giant Spin-Charge Conversion at a Rashba Oxide Interface with a Strongly Correlated Metal Interlayer

The two-dimensional electron gas (2DEG) formed at interfaces between SrTiO<sub>3</sub> and other oxide insulating layers is promising for the efficient spin-charge conversion due to the large Rashba spin-orbit interaction (RSOI). However, these insulating layers prevent the propagation of a spin current. Here, using a strongly correlated metal LaTiO<sub>3+δ</sub> and the 2DEG at the LaTiO<sub>3+δ</sub>/SrTiO<sub>3</sub> interface, we demonstrate giant spin-charge conversion efficiencies up to ~190 nm. Our results suggest that the on-site Coulomb repulsion in LaTiO<sub>3+δ</sub> and the giant RSOI of LaTiO<sub>3+δ</sub>/SrTiO<sub>3</sub> are the key to efficient spin-charge conversion. Our findings highlight the possibilities of oxide interfaces for spin-orbitronics applications.

Interconversion phenomena between charge and spin currents at material interfaces have attracted much attention because of their potential application in the highly efficient control of magnetization in next-generation spin-orbitronics devices. The spin-charge conversion at interfaces, the so-called inverse Edelstein effect (IEE), mainly originates from the Rashba spin-orbit interaction (RSOI) induced by the broken spatial inversion symmetry of interfaces. At material interfaces, the RSOI resolves the spin degeneracy of the electronic band, splitting it into up- and down-spin bands. In the simple single parabolic band picture shown in Fig. 1(a), the Fermi surface splits into large and small circles. When a spin current is injected into these bands, the chemical potential of up-spin electrons increases, while that of down-spin electrons decreases (top of Fig. 1(a)). Thus, the large and small Fermi surfaces shift in opposite directions, and electrons move to the right overall (bottom of Fig. 1(a)), resulting in a spin-charge conversion. Large spin-charge current conversion has been observed in the two-dimensional electron gas (2DEG) formed at interfaces between perovskite-oxide SrTiO<sub>3</sub> (STO) and other oxides, such as LaAlO<sub>3</sub> (LAO) and AlO<sub>x</sub> [1–5]. However, both LAO and AlO<sub>x</sub> are insulators, which hamper the direct transport of the spin current, preventing the full potential of 2DEG at the STO interface.

The 2DEG formed at the metal LaTiO<sub>3+δ</sub> (LTO)/insulator STO interface is an alternative candidate. Although LTO is a strongly correlated Mott insulator, it usually transitions to a metal due to slight excess oxygen or lattice distortion. This metallic nature of LTO is desirable for the efficient transport of the spin current. Furthermore, unlike ordinary metals, in which itinerant *s,p* carriers dominate transport, LTO has only up-spin electrons of the relatively localized *d* orbital on a Ti site at the Fermi level. The down-spin states exist far above the Fermi level due to the strong on-site Coulomb repulsion of the strongly correlated system. Thus, significant suppression of spin scattering during spin-current transport is expected. Therefore, the LTO/STO interface is expected to be an ideal stage for efficient spin-charge conversion. We can incorporate a coherently grown single-crystal LTO layer into perovskite-oxide heterostructures due to their excellent lattice matching. However, growing high-quality LTO is generally difficult because LTO easily changes to the La<sub>2</sub>Ti<sub>2</sub>O<sub>7</sub> phase. Here, by carefully growing a high-quality all-epitaxial La<sub>0.67</sub>Sr<sub>0.33</sub>MnO<sub>3</sub> (LSMO) (12 nm)/LTO (1.2 nm)/STO heterostructure by molecular beam epitaxy (MBE) (Fig. 1(b)), we have demonstrated giant spin-charge conversion efficiency  $\lambda_{\text{IEE}}$  values, up to ~190 nm, at the LTO/STO interface [6]. By combining resonant angle-resolved photo-



**Figure 1:** Inverse Edelstein effect and sample structure. (a) Schematic illustration of the inverse Edelstein effect in a single parabolic-band model. RSOI resolves the spin degeneracy of the electronic band and splits it into up- and down-spin bands (orange and blue curves). The Fermi surface splits into large and small circles with opposite spin chirality (arrows). When a spin current is injected into these bands, the chemical potential of the up-spin electrons increases (filled orange circles), while that of the down-spin electrons decreases (open blue circles) [top figure of (a)]. Thus, the large and small Fermi surfaces shift in opposite directions. Due to the difference in the size of the circles, the movement of the outer circle is dominant, and in total, the electrons move toward the right side [bottom of (a)], resulting in spin-to-charge conversion. (b) Schematic structure of the LSMO/LTO/STO sample used for spin pumping measurements. (c) Summary of the temperature dependences of  $\lambda_{\text{IEE}}$  in various material systems with theoretically calculated  $\lambda_{\text{IEE}}$ .

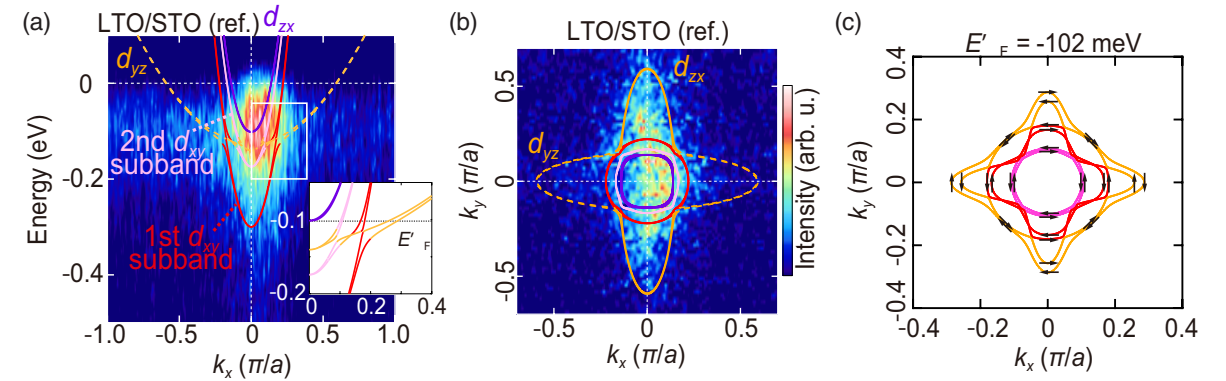


**Figure 2:** R-ARPES measurement results for the band dispersion and Fermi surface with the theoretical curves and spin orientations, and a comparison between the experimental  $\lambda_{\text{IEE}}$  and theoretical  $\lambda_{\text{IEE}}$ . (a) Band dispersion of a reference sample LTO (1.2 nm)/STO along the wave vector  $k_x$  in the  $x$  direction (current direction) measured by R-ARPES. The 2DEG states are observed using the resonant photon energy for the Ti  $L_3$  absorption edge of the  $\text{Ti}^{3+}$  component ( $h\nu = 459.7$  eV). The solid and broken curves represent the band dispersions calculated by the effective tight-binding model. The inset is the enlarged band dispersion near the crossing point of the  $d_{xy}$  and  $d_{xz}$  bands. The dotted line of the inset corresponds to the Fermi level used for the calculation of  $\lambda_{\text{IEE}}$  in the LSMO/LTO/STO sample ( $E_F = -102$  meV). Here,  $E_F$  and  $E_F$  are the Fermi levels of LTO/STO obtained by the R-ARPES measurement and the Hall effect measurement, respectively. (b) Fermi surface of the reference sample LTO (1.2 nm)/STO obtained by R-ARPES. Although it is not clear, the Fermi surface of the thin LTO layer, which is considered to be small due to its small carrier concentration, may be partially overlapped with the Fermi surface of the 2DEG at around the center of the  $k_x$ - $k_y$  plane. In this measurement, the Fermi surface elongated in the  $k_y$  direction is visible, but the surface elongated in the  $k_x$  direction is almost not, due to the experimental geometry of the ARPES measurements. The solid and broken curves are the Fermi surfaces calculated by the effective tight-binding model at  $E_F = 0$  meV. (c) Calculated Fermi surface and spin expectation values (arrows) at  $E_F = -102$  meV by the effective tight-binding model. The orange, red, and pink lines are  $d_{yz}/d_{xx}$ , first  $d_{xy}$ , and second  $d_{xy}$  bands, respectively.

emission spectroscopy (R-ARPES) measurements and theoretical calculations, we have clarified the origin of large  $\lambda_{\text{IEE}}$  at the LTO/STO interface.

To evaluate  $\lambda_{\text{IEE}}$  in the 2DEG at the LTO/STO interface, we conducted spin pumping measurements using ferromagnetic resonance, in which the spin current was injected from LSMO and converted into a current in the 2DEG. As shown in Fig. 1(c), we show our data for  $\lambda_{\text{IEE}}$  as a function of temperature ( $T$ ) along with the data reported for various STO interfaces with other materials. Here, we obtained a large  $\lambda_{\text{IEE}}$  of 193.5 nm at 15 K, showing the superiority of the LTO/STO systems.

To clarify the role of the multi-orbital band structure in the IEE, we carried out a theoretical calculation based on an effective tight-binding model. We optimized the band parameters so that the calculation reproduces the band dispersion measured by R-ARPES for the reference sample LTO (1.2 nm)/STO shown in Figs. 2(a) and (b). In addition to spin-orbit coupling, the complex hybridization of these bands generates a Rashba effect with large spin splitting (inset in Fig. 2(a)). The theoretical band dispersion and Fermi surface agree with the R-ARPES results (Figs. 2(a), (b)). From this calculation result, we theoretically derived  $\lambda_{\text{IEE}}$  (Fig. 1(c)). In Fig. 1(c), the calculated results reproduce the experimental  $\lambda_{\text{IEE}}$  values well. The Fermi surface shows large Rashba splitting (Fig. 2(c)), which is thought to be one of the main causes of the large  $\lambda_{\text{IEE}}$ . The large  $\lambda_{\text{IEE}}$  values obtained in our study also suggested that the metallicity and the correlated transport with a large Coulomb repulsion of LTO likely play significant roles in spin current transport and in the enhancement of  $\lambda_{\text{IEE}}$ .

In summary, we have obtained an extremely large

$\lambda_{\text{IEE}}$  of up to ~190 nm using 2DEG at the LTO/STO interface. The coexistence of highly efficient spin-current transport and spin-current conversion in LTO/STO highlights the physical phenomena in spin-orbitronics, and paves the way for ultralow-power computing and storage by spintronic devices.

### REFERENCES

- [1] E. Lesne, Y. Fu, S. Oyarzun, J. C. Rojas-Sánchez, D. C. Vaz, H. Naganuma, G. Sicoli, J. -P. Attané, M. Jamet, E. Jacquet, J. -M. George, A. Barthélémy, H. Jaffrès, A. Fert, M. Bibes and L. Vila, *Nat. Mater.* **15**, 1261 (2016).
- [2] S. Ohya, D. Araki, L. D. Anh, S. Kaneta, M. Seki, H. Tabata and M. Tanaka, *Phys. Rev. Res.* **2**, 012014(R) (2020).
- [3] D. C. Vaz, P. Noël, A. Johansson, B. Göbel, F. Y. Bruno, G. Singh, S. McKeown-Walker, F. Trier, L. M. Vicente-Arche, A. Sander, S. Valencia, P. Bruneel, M. Vivek, M. Gabay, N. Bergeal, F. Baumberger, H. Okuno, A. Barthélémy, A. Fert, L. Vila, I. Mertig, J. -P. Attané and M. Bibes, *Nat. Mater.* **18**, 1187 (2019).
- [4] P. Noël, F. Trier, L. M. V. Arche, J. Bréhin, D. C. Vaz, V. Garcia, S. Fusil, A. Barthélémy, L. Vila, M. Bibes and J. -P. Attané, *Nature* **580**, 483 (2020).
- [5] J. -Y. Chauleau, M. Boselli, S. Gariglio, R. Weil, G. de Loubens, J. -M. Triscone and M. Viret, *Europhys. Lett.* **116**, 17006 (2016).
- [6] S. Kaneta-Takada, M. Kitamura, S. Arai, T. Arai, R. Okano, L. D. Anh, T. Endo, K. Horiba, H. Kumigashira, M. Kobayashi, M. Seki, H. Tabata, M. Tanaka and S. Ohya, *Nat. Commun.* **13**, 5631 (2022).

### BEAMLINER

BL-2A

S. Kaneta-Takada<sup>1</sup>, M. Kitamura<sup>2</sup>, S. Arai<sup>1</sup>, T. Arai<sup>1</sup>, R. Okano<sup>1</sup>, L. D. Anh<sup>1</sup>, T. Endo<sup>1</sup>, K. Horiba<sup>2</sup>, H. Kumigashira<sup>2,3</sup>, M. Kobayashi<sup>1</sup>, M. Seki<sup>1</sup>, H. Tabata<sup>1</sup>, M. Tanaka<sup>1</sup> and S. Ohya<sup>1</sup> (<sup>1</sup>The Univ. of Tokyo, <sup>2</sup>KEK-IMSS-PF, <sup>3</sup>Tohoku Univ.)